ACS Catalysis

Research Article

pubs.acs.org/acscatalysis

Nickel–Iron Alloy Supported over Iron–Alumina Catalysts for Steam Reforming of Biomass Tar Model Compound

J. Ashok and S. Kawi*

Department of Chemical and Biomolecular Engineering, National University of Singapore, Singapore 119260, Republic of Singapore

ABSTRACT: Iron–alumina-supported nickel–iron alloy catalysts were tested in a fixed-bed reactor for steam reforming of toluene as a biomass tar model compound. The influence of the calcination temperature of the iron–alumina support was also explored for the steam reforming reaction. Ni supported on an Fe_2O_3–Al_2O_3 support calcined at 500 °C [NFA(500)] gave superior catalytic performance in terms of activity and stability over other catalysts. NFA(500) gave a toluene conversion of more than 90% for a period of 26 h with a H_2/CO value of 4.5. According to XRD analysis, the Ni–Fe alloys were formed and stable throughout the reforming reaction. It was observed from XPS results that the surface of the reduced NFA(500) catalyst was enriched with Fe species, where the other catalysts were enriched with Ni species. These surface Fe species play the role of cocatalysts by increasing the coverage of oxygen species during the reforming reaction to enhance the reaction of toluene and suppresses coke formation. The presence of oxygen species in the reduced catalysts was confirmed by temperature-programmed surface reaction (TPSR) with toluene and water over NFA catalysts. A temperature-programmed oxidation (TPO) study on spent catalysts revealed that the NFA(500) and NFA(700) catalysts have an additional low-temperature oxidation peak at around 525 and 535 °C, respectively, suggesting the presence of a higher amount of amorphous carbon compared with the NFA(900) catalyst. The presence of a low-temperature oxidation peak at 525 °C for the NFA(500) catalyst is one of the reasons for its stable catalytic performance compared with other catalysts.

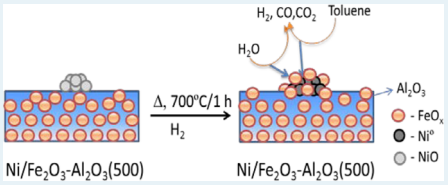

KEYWORDS: *hydrogen production, nickel–iron alloy, biomass, toluene steam reforming, iron–alumina*

1. INTRODUCTION

Catalytic steam reforming of biomass tar to produce H_2-rich synthesis gas is becoming more attractive because of the rising interest in utilizing biomass—derived from forest, agricultural, and municipal solid waste materials—as a renewable energy source.[1−5] However, one of the most critical problems in utilization of biomass via the gasification process is the formation of tars, an undesirable reaction that is an impediment to the commercialization of the biomass gasification process. In addition, these tars are largely aromatic hydrocarbons, such as benzene, toluene, and naphthalene, which harness large amounts of energy, thereby lowering the energy content of the product gas. These tars also cause operational problems when cooled and condensed in heat exchangers, lowering heat transfer efficiencies, plugging pipes, and so on. Therefore, conversion of biomass tars is crucial in the biomass gasification process. Among many processes, catalytic steam reforming of biomass tar is a considerably attractive approach for tar removal during biomass gasification since it produces syngas, which is a high-value gas product.[6−8]

In steam reforming of tar, the catalysts should exhibit high catalytic performance in terms of catalyst stability and high resistance toward coke deposition.[9,10] It has been known from the literature that supported metal (e.g., Ni, Co, Pt, Pd) catalysts are effective for steam reforming of biomass tar.[11−16] Moreover, Ni-based catalysts have been widely investigated for the steam reforming of biomass tar because of its low cost and high activity.[7] In the development process of highly active and stable Ni-based catalysts, the effects of supports, additives, oxides, and other metals on Ni-based systems have been investigated.[17,18] However, the development of a cheap, stable, and coke-resistant catalyst for steam reforming of tar remains as a challenge for many researchers. In a bid to reduce the cost of the catalyst, alumina (Al_2O_3) has been used as the catalyst support for Ni-based systems in many instances. However, the main drawback of Ni/Al_2O_3 catalysts lies in the rapid catalyst deactivation that occurs because of the encapsulation of carbon and sintering or loss of the active Ni component at high temperature.[19,20] It is also reported that the addition of CeO_2 to Ni catalysts enhances the catalytic performance by forming a Ni–CeO_2 nanocomposite. Good catalytic activity and high resistance toward formation of coke were attributed to the existence of the large interface between the Ni metal and the Ce oxide surface.[21] Similar to this work, we recently explored Ni supported on CeO_2-doped CaO–Al_2O_3 as a catalyst for steam reforming of toluene and observed that the addition of CeO_2 to Ni/CaO–Al_2O_3 in an optimum quantity can significantly enhance the steam reforming performance. As reported earlier,[10] the promotional effect of CeO_2 is mainly due to its redox properties as well as the fact that Ce oxide species can interact with Ni species to form Ni–CeO_2 nanocomposites.

Furthermore, alloying Ni[22−24] with other metals can improve the catalytic performance in terms of activity and stability, and one such suitable modifier is Fe. In addition, like Ce species, Fe

Received: July 30, 2013
Revised: October 17, 2013
Published: November 7, 2013

species have good redox properties. It has also been reported that the improved performance in the steam reforming activity of Ni−Fe/Al_2O_3 catalysts is due to the presence of an intimate interaction between Fe and Ni, which results in the formation of a Ni−Fe alloy. As has been reported,[22] in the Ni−Fe/Al_2O_3 catalytic system, Fe plays the role of a cocatalyst. Since Fe has a higher oxygen affinity than Ni,[25] the addition of Fe to Ni catalysts can increase the coverage of oxygen atoms during the steam reforming reactions. This increment in oxygen coverage suggests that Ni−Fe alloy species are vital in enhancing the performance in steam reforming of tar. In addition, was also recently reported that the presence of uniform Ni−Fe alloy particles in Ni−Fe/Mg/Al catalysts enables a high catalytic performance in the steam reforming of toluene and phenol.[24] Thus, obtaining an intimate interaction between Ni and Fe species to form Ni−Fe alloys is a crucial entity in preparing Ni−Fe-based catalysts. Hence, in the present study, in order to obtain an intimate interaction between most of the Ni species and the Fe species in the Ni/Fe_2O_3−Al_2O_3 catalyst system, we first synthesized Fe_2O_3−Al_2O_3 support materials by a coprecipitation method and subsequently calcined them at different temperatures in order to establish different kinds of interactions between Fe and Al species present in the supports. We chose to synthesize the Fe_2O_3−Al_2O_3 support materials first because according to previous reports,[26] the redox properties and thermal stability of Fe oxides can increase significantly in the presence of Al oxides. In all of the support materials, the Fe to Al molar ratio was kept constant. This Fe_2O_3−Al_2O_3 support was used to prepare Ni/Fe_2O_3−Al_2O_3 catalysts by the impregnation method. The thus-prepared Ni/Fe_2O_3−Al_2O_3 catalysts were used to obtain FeO_x−Al_2O_3-supported Ni−Fe alloy catalysts upon reductive pretreatment with H_2 gas at 700 °C for 1 h to investigate their catalytic performance for the toluene steam reforming process at a reaction temperature of 650 °C and ambient pressure.

In steam reforming of toluene (SRT), the final products can be regarded as the result of competition of many parallel and consecutive reactions.[27] However, different operation conditions such as the steam-to-carbon (S/C) ratio, temperature, and catalysts will result in different products. These evolutions of gases yields under different conditions can be explained by the following reactions involved in toluene steam reforming.

steam reforming:

$$C_7H_8 + 7H_2O \rightarrow 7CO + 11H_2 \quad (1)$$

steam reforming:

$$C_7H_8 + 14H_2O \rightarrow 7CO_2 + 18H_2 \quad (2)$$

water-gas shift:

$$CO + H_2O \rightarrow CO_2 + H_2 \quad (3)$$

dry reforming:

$$C_7H_8 + 7CO_2 \rightarrow 14CO + 4H_2 \quad (4)$$

hydrodealkylation:

$$C_7H_8 + H_2 \rightarrow C_6H_6 + CH_4 \quad (5)$$

steam dealkylation:

$$C_7H_8 + H_2O \rightarrow C_6H_6 + CO + 2H_2 \quad (6)$$

steam dealkylation:

$$C_7H_8 + 2H_2O \rightarrow C_6H_6 + CO_2 + 3H_2 \quad (7)$$

steam reforming of methane:

$$CH_4 + H_2O \rightarrow CO + 3H_2 \quad (8)$$

Other reactions such as carbon formation by toluene decomposition and cracking are also included in the process.

2. EXPERIMENTAL SECTION

2.1. Catalyst Preparation. Fe_2O_3−Al_2O_3 mixed oxides with the nominal Fe:Al molar ratio of 1:2 were prepared using a coprecipitation method. In a typical preparation method, nearly saturated solutions of nitrates (ferric nitrate and aluminum nitrate) were homogeneously mixed in the required molar ratios. The pH value of the solution was then slowly adjusted to ∼10 with 2 M aqueous ammonia solution, and the solution was then stirred continuously for another 1 h to complete the precipitation process. The precipitated solution was dried in an oven at 100 °C for 24 h and then calcined at different temperatures (500, 700, and 900 °C) over 4 h in an air atmosphere. The as-prepared catalyst supports were labeled as FA(x), where x represents the calcination temperature of the support.

The 10 wt % Ni supported catalysts were prepared by a simple wetness impregnation method wherein an aqueous solution containing the required amount of $Ni(NO_3)_2{\cdot}6H_2O$ was mixed with the requisite amount of support material to yield the respective Ni weight percent needed. The mixtures were then dried under constant stirring at 80 °C and further dried at 100 °C for another 24 h before they were calcined in air at 700 °C for 4 h (under a ramping rate of 3 °C/min). The thus-prepared catalysts were labeled as NFA(x), where x represents the calcination temperature of the Fe_2O_3−Al_2O_3 support material.

2.2. Catalyst Characterization. The X-ray diffraction (XRD) pattern of each catalyst was measured on a Shimadzu XRD-6000 diffractometer using Cu Kα radiation. The catalyst was placed on an aluminum slide and scanned from 2θ of 20° to 80° at a ramp rate of 2°/min. The beam voltage and current used were 40 kV and 30 mA, respectively. H_2/CO Temperature-programmed reduction (TPR) measurements for fresh catalysts were performed on a Quantachrome ChemBET-3000 instrument. Prior to the TPR measurement, 0.04 g of catalyst was outgassed in He for 1 h at 300 °C to remove any moisture and then cooled to room temperature. Then 5% H_2/N_2 or 5% CO/He gas was introduced to the catalyst while the temperature of the furnace was increased at a heating rate of 10 °C/min to 1000 °C. The CO chemisorption was done in the Quantachrome ChemBET-3000 instrument. Prior to the CO pulse chemisorption measurement, the sample was reduced at 700 °C for 1 h under H_2 gas before it was cooled to 0 °C in a helium flow of 80 mL/min. The CO chemisorption was measured at 0 °C by introducing pulses of CO using 5% CO/He with a loop volume of 250 μL. The pulses were continued until no further uptake of CO was measured.

In order to understand the actual reduced species involved in the SRT reaction, the following characterization experiments were conducted in sequence: (1) H_2 temperature-programmed reduction (H_2-TPR_1), (2) temperature-programmed oxidation (TPO), and (3) temperature-programmed reduction (H_2-TPR_2). In these experiments, 5% H_2/N_2 and 5% O_2/N_2 were used for the TPR and TPO steps, respectively, while the

dx.doi.org/10.1021/cs400621p | ACS Catal. 2014, 4, 289−301

temperature of the system was increased from room temperature to 700 °C at a ramp rate of 10 °C/min and dwelled for 1 h. These experiments were performed on the Quantachrome ChemBET-3000 instrument. For temperature-programmed surface reaction (TPSR) experiments with toluene and water, about 30 mg of catalyst sample was loaded in an isothermal zone of the reactor. Prior to the TPSR measurement, the catalyst was reduced in H_2 gas at 700 °C for 1 h. After the sample was cooled to room temperature, the H_2 gas was switched to 80 mL/min of He gas saturated with toluene/water at room temperature, and the temperature was increased to 800 °C at a rate of 10 °C/min. The reactor effluent gas was analyzed by mass spectroscopy (Thermostat GSD300).

The catalyst surface analysis was performed using X-ray photoelectron spectroscopy (XPS) from a KRATOS AXIS Hsi 165 spectrometer equipped with a Mg Kα source (1253.6 eV). The total amount of deposited carbon on the spent catalysts was measured using thermogravimetric analysis (TGA) on a Shimadzu DTG-60 thermogravimetric analyzer. About 10 mg of spent catalyst was used in each TGA experiment and was heated in air to 1000 °C at a heating rate of 10 °C/min. The type of carbon deposited on spent catalysts was determined by TPO, in which about 10 mg of spent sample was heated in an 80 mL/min flow of 5% O_2/N_2 at a rate of 10 °C/min up to 900 °C and held at this temperature for 15 min. The amount of CO_2 emission as a function of temperature was recorded using mass spectroscopy (Thermostat GSD300).

2.3. Catalyst Evaluation. The catalytic reaction was carried out in a fixed-bed quartz reactor with an inner diameter of 4 mm and a length of 400 mm as reported previously.[28,29] The catalyst in each test was held by quartz wool placed in the middle of the reactor. The operating conditions were as follows: catalysts amount = 0.03 or 0.10 g; toluene amount = 0.19 mmol (diluted by He gas); S/C ratio = 1.0 to 4.0; reaction temperature = 650 °C. Prior to the catalytic reaction, the catalyst was reduced in 30 mL/min H_2 at 700 °C for 1 h and then purged in 120 mL/min helium while the temperature reached the desired reaction temperature (650 °C). Water and toluene were vaporized at 300 °C in a preheater and mixed with 120 mL/min He gas before entering the main reactor in the vapor state. The reaction products were then passed through a cold trap at a temperature of 5 °C to condense the unreacted water from the gasification reaction. The noncondensable gas product was analyzed using a gas chromatograph (HP 6890) equipped with a Carboxen column and a thermal conductivity detector (TCD). The chromatogram showed peak areas for all of the reacted gases, which were then converted to volume percent using a calibration curve. The total flow rate of the product gases was measured using a bubble flow meter. The conversion of toluene was expressed in terms of carbon conversion, which was calculated using the following formula:

$$X_{\text{toluene}} = \frac{n_{\text{CO}} + n_{\text{CO}_2}}{7n_{\text{r in}}} \times 100\,\% \tag{9}$$

where n_j is the molar flow rate of gas j.

3. RESULTS AND DISCUSSION

3.1. Catalyst Activity and Stability Study. *3.1.1. Steam Reforming of Toluene over NFA Catalysts.* The catalytic performance for steam reforming of toluene as a biomass tar model compound was carried out in a continuous fixed-bed reactor over 10 wt % Ni supported on Fe_2O_3–Al_2O_3 supports calcined at different temperatures. Table 1 presents the product gas distributions, H_2/CO molar ratios, and catalytic performances for NFA catalysts after 1 h reaction time. The reaction was performed at 650 °C with an S/C ratio of 3.4 as reported earlier.[28,29] In the blank test there was no conversion of toluene at all, showing that presence of catalyst is very important for this reaction. In this SRT process, the main product stream consists of H_2, CO, CO_2, and trace amounts of CH_4 (<1%). The production of these gases can be explained by eqs 1 to 4. According to Table 1, the toluene conversions for the NFA(500), NFA(700), and NFA(900) catalysts were 80.9, 68.2, and 48.7%, respectively. It was also observed that the H_2, CO, and CO_2 yields increased correspondingly with increasing toluene conversion. In comparison, NFA(500) and NFA(700) produced significantly a higher H_2/CO value of ~3.2 compared with the NFA(900) catalyst's H_2/CO value of 1.8. This is a result of the fact that the NFA(500) and NFA(700) catalysts have higher amounts of available lattice oxygen species (to be shown later from TPSR of toluene results), which apparently promotes the water-gas shift (WGS) reaction (eq 3). Next, the time-dependent catalytic performance of NFA catalysts for 6 h reaction time is depicted in Figure 1, which shows that the overall catalytic performance of the NFA catalysts was influenced by the calcination temperature of the catalyst support, as the catalyst support calcined at lower temperature of 500 °C, NFA(500), showed superior catalytic performance compared with the others. It can also be observed from Figure 1 that all of the catalysts showed a decreasing trend of catalytic performance with time on stream. This decrease in catalytic performance with time is primarily due to the deposition of carbon species over the catalysts during the SRT process at 650 °C. This deposited carbon can encapsulate the active metal species, resulting in a decrease in the amount of catalytically active species. The nature and amount of carbon species deposited over spent NFA catalysts were characterized, and the same will be discussed in later parts of this article. In addition, structural changes within the NFA catalysts during the SRT process can also play an important role in their catalytic performance with time on stream. These structural changes were identified by characterizing reduced and spent NFA catalysts, and the obtained results will also be discussed later in this article.

Table 1. Catalytic Performance of NFA(x) Catalysts after 1 h Reaction Time[a]

catalyst	toluene conversion (%)	product distribution (μmol min^{-1}) H_2	CO	CO_2	H_2/CO
blank	–	–	–	–	–
NFA(500)	80.9	1641.7	521.8	521.4	3.1
NFA(700)	68.2	1426.4	423.7	487.8	3.3
NFA(900)	48.7	743.2	419.7	153.1	1.8

[a]Reaction conditions: toluene = 188 μmol min^{-1}; steam = 4444 μmol min^{-1}; He = 5357 μmol min^{-1}; W = 30 mg; reaction temperature = 650 °C; reaction time = 1 h.

3.1.2. Effect of Steam Feed Concentration. The influence of the steam-to-carbon ratio on the catalytic activity of NFA catalysts was investigated by varying the S/C ratio from 1.0 to 4.0 at a reaction temperature of 650 °C after 1 h reaction time on stream. The obtained results are depicted in Figure 2, which

dx.doi.org/10.1021/cs400621p | ACS Catal. 2014, 4, 289–301

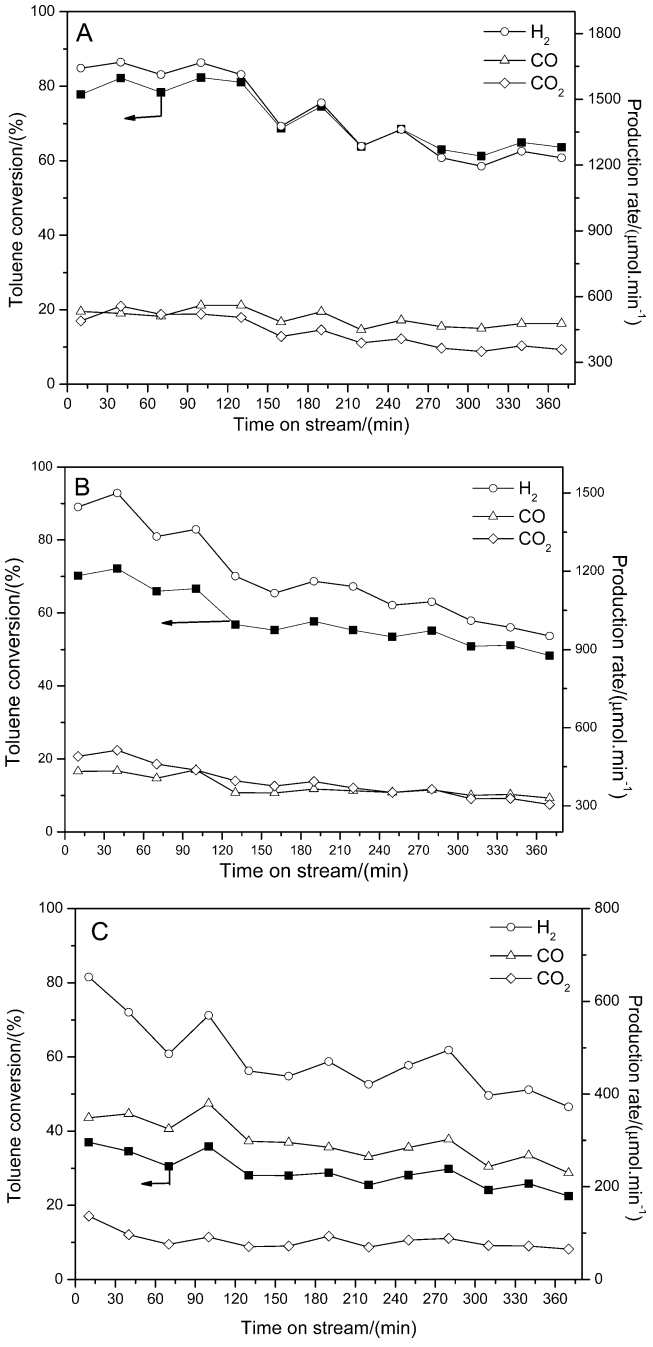

Figure 1. SRT performance of (A) NFA(500), (B) NFA(700), and (C) NFA(900) catalysts. Reaction conditions: toluene = 188 μmol min^{-1}; steam = 4444 μmol min^{-1}; He = 5357 μmol min^{-1}; W = 30 mg; reaction temperature = 650 °C.

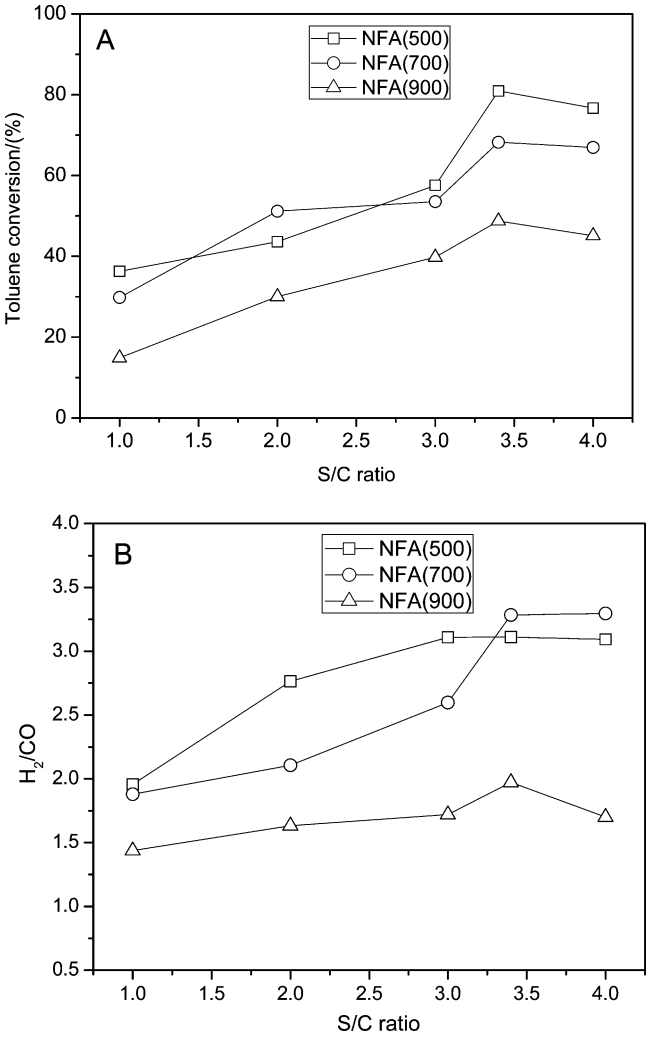

Figure 2. Effect of steam-to-carbon ratio on the catalytic performance of NFA catalysts: (A) toluene conversion (%); (B) H_2/CO ratio. Reaction conditions: toluene = 188 μmol min^{-1}; He = 5357 μmol min^{-1}; W = 30 mg; reaction temperature = 650 °C; reaction time = 1 h.

shows that the S/C ratio has a significant influence on the catalytic activity and the distribution of the products. From Figure 2 it can also be observed that all of the catalysts display similar behaviors with varying S/C ratio—increasing toluene conversion and H_2/CO ratio with increasing S/C ratio—despite achieving different conversions and product yields. Ideal SRT reactions at S/C ratios of 1 and 2 are shown in eqs 1 and 2, respectively. Equation 3 represents the WGS reaction to produce CO_2 and more H_2. The CO_2 produced by eqs 2 and 3 may react with toluene according to dry reforming of toluene (eq 4). A comparison of the obtained results (Table 1, Figure 1, and Figure 2) and the above possible reactions clearly shows that even at an S/C ratio of 2 or more, the toluene reforming reaction did not proceed according to eq 2. Instead, it is more appropriate to postulate that it proceeds according to SRT with an S/C ratio of 1 (eq 1) followed by the WGS reaction (eq 3). This suggests that increasing the steam amount in the feed can enhance the SRT reaction by enhancing the WGS reaction to produce more H_2 gas. High amounts of H_2 and CO_2 were produced at high S/C ratios via the WGS reaction since a high steam partial pressure pushes the WGS equilibrium toward formation of H_2 and CO_2. Furthermore, an excess of steam is known to be beneficial to the suppression of coking because it leads to partial gasification of the carbon formed.[30] In Figure 2, when the S/C ratio was raised to 3.4, the conversion of toluene reached a maximum for all of the catalysts and is almost similar to that with an S/C ratio of 4. Likewise, the product yield with respect to the H_2/CO value also reached a maximum at an S/C ratio of 3.4 (Figure 2 B). This indicates that increasing H_2O beyond an optimum content not only promotes steam reforming of toluene but also substantially favors the water-gas shift reaction. Domine et al.[31] investigated the effect of the S/C ratio on hydrogen production over Pt and Rh noble-metal-

dx.doi.org/10.1021/cs400621p | ACS Catal. 2014, 4, 289−301

based catalysts. They concluded that the effect of the S/C ratio depends on the nature of the metal sites on the catalyst. It is evident from Figure 2 that an S/C ratio of 3.4 is optimum for all of the NFA catalysts to attain their best toluene reforming performances at a reaction temperature of 650 °C.

3.1.3. Catalyst Stability Study. In order to integrate this system with the industrial reforming process downstream, the catalysts should be capable of completely reforming toluene to H_2, CO, and CO_2 by preventing possible coke deposition in the SRT reformer at ambient temperatures. Therefore, the following severe experimental conditions were imposed to examine the stability of the NFA catalysts for the SRT reaction: toluene = 0.19 mmol (diluted by He gas); S/C ratio = 3.4; reaction temperature = 650 °C; space velocity = 132 L g^{-1} h^{-1} at 25 °C. Figure 3A,B displays the conversion of toluene and the product selectivities (H_2/CO ratio), respectively, as functions of reaction time. It is observed that the NFA(500) and NFA(700) catalysts exhibited good activity and stability under the present operating conditions. The NFA(500) catalyst was able to maintain toluene conversion at a level of more than 90% for a period of 26 h reaction time. In contrast, the NFA(700) catalyst attained a toluene conversion of more than 90% for ca. 20 h, with a subsequent gradual decrease in toluene conversion as time proceeds. Eventually, a toluene conversion of 85% after 26 h reaction time was obtained for the NFA(700) catalyst. In stark contrast to the other catalysts, the NFA(900) catalyst showed toluene conversion ranging from 75 to 40% over a 20 h run time. The H_2/CO values for the NFA catalysts (Figure 3B) decrease in the order NFA(500) > NFA(700) > NFA(900). This suggests that the NFA(500) catalyst showed superior SRT catalytic performance in terms of conversion, stability, and H_2/CO value for ca. 26 h reaction time compared with the NFA(700) and NFA(900) catalysts.

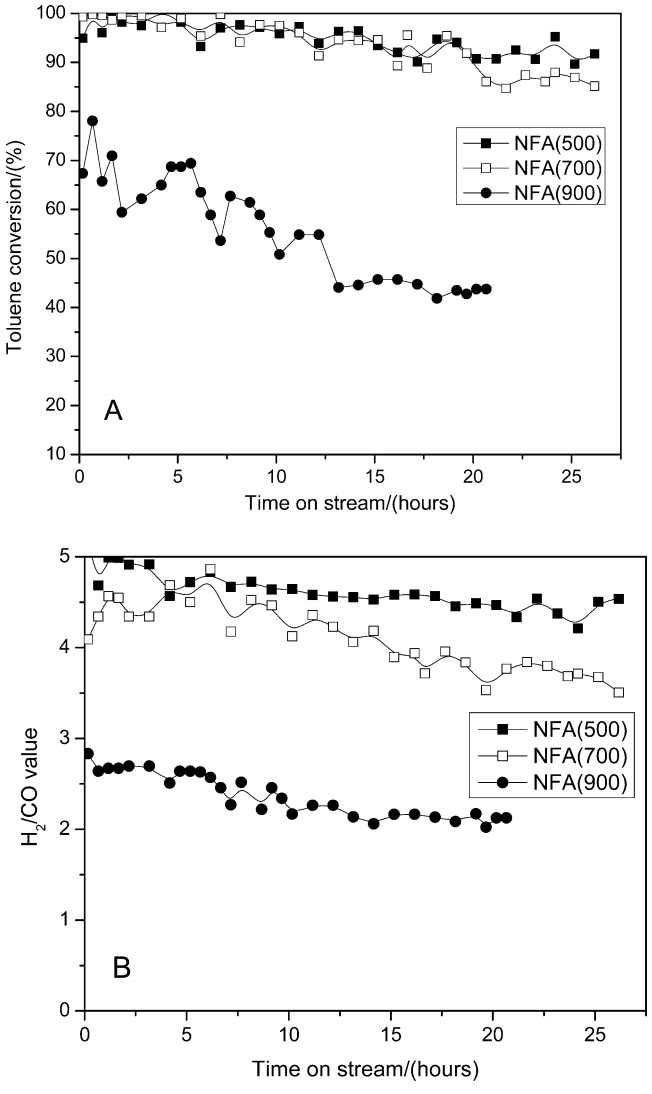

Figure 3. Stability study for steam reforming of toluene over Fe_2O_3–Al_2O_3-supported Ni catalysts: (A) toluene conversion and (B) H_2/CO values against time on stream. Reaction conditions: toluene = 188 μmol min^{-1}; steam = 4444 μmol min^{-1}; He = 5357 μmol min^{-1}; W = 100 mg; reaction temperature = 650 °C.

3.2. Characterizations of Fresh and Spent Catalysts.

3.2.1. DT/TG Analyses of Oven-Dried Fe–Al Support. To understand the potential transformation of the oven-dried Fe_2O_3–Al_2O_3 support precursor in the muffle furnace, TGA and differential thermal analysis (DTA) were performed up to 1000 °C at a heating rate of 10 °C/min under an air atmosphere, as shown in Figure 4. The DTA trace in Figure 4 shows four endothermic peaks. The initial endothermic peak (~90 °C) indicates loss of physisorbed water present in the precursor, while the other three endothermic peaks (130, 170, and 272 °C) represent both weight loss and formation of gaseous species that are caused by decomposition reactions occurring in various distinguishable steps.[32] The sample undergoes three decomposition steps in the temperature range of 120–320 °C, as evidenced by the huge sample weight loss, sharp endothermic effect, and vigorous gas emissions (NH_3, NO_x, and H_2O). The TGA curve presented in Figure 4 shows that as the temperature was increased from ambient temperature to around 300 °C, the weight of the oven-dried Fe–Al support precursor decreased from 8.79 to 2.3 mg. This major weight loss of 73% denotes that most of the precursor decomposed below 300 °C to form various oxides. Furthermore, a significant weight loss of >6% was recorded as the temperature was increased from 300 °C to around 500 °C, and there was no substantial weight loss (<2%) observed above 500 °C. The weight loss up to 1000 °C agrees well with the theoretical value corresponding to complete decomposition to Fe_2O_3 and Al_2O_3. The aforementioned results suggest that a

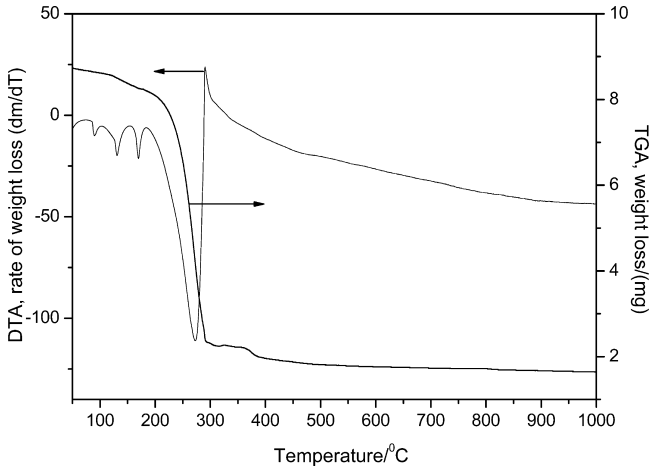

Figure 4. DTA and TGA of the oven-dried Fe_2O_3–Al_2O_3 catalyst support precursor.

dx.doi.org/10.1021/cs400621p | ACS Catal. 2014, 4, 289–301

minimum temperature of 500 °C is required to prepare a stable Fe_2O_3–Al_2O_3 support material.

3.2.2. Surface Area Analysis. Table 2 shows the Brunauer–Emmett–Teller (BET) surface areas of bare supports and supported Ni catalysts. The surface area of the bare FA support was observed to be greatly reduced with increasing support calcination temperature because of sintering of the support.[33] It was also observed that the supported Ni catalysts have lower surface areas than the bare FA supports. This is primarily due to the penetration of the active component into the pores of the support during the preparation, which in turn results in the dispersion of the active component on the support. This decrease in surface area is greater for NFA(500) than for the other catalysts because its corresponding FA support was calcined at a lower temperature (i.e, 500 °C). The highest surface area of 93 m^2/g for the NFA(500) catalyst is possibly one of the reasons for its superior catalytic performance compared with the other catalysts.

Table 2. BET Surface Areas and H_2 Consumption and CO Uptake Values for FA and NFA Catalysts

sample	A_{BET} (m^2/g)	H_2 consumption (mmol/g)[a]	H_2 consumption (mmol/g)[b]	CO uptake (μmol/g_{cat})[c]
FA(500)	169.8	–	–	–
NFA(500)	93.4	8.98	10.06	19.15
FA(700)	92.4	–	–	–
NFA(700)	81.1	9.31	10.24	18.23
FA(900)	20.3	–	–	–
NFA(900)	15.1	9.95	10.52	15.97

[a]H_2 consumption below 700 °C in TPR_1 profiles shown in Figure 7. [b]H_2 consumption below 700 °C in TPR_2 profiles shown in Figure 7. [c]Obtained from CO pulse chemisorption at 0 °C.

3.2.3. XRD Analysis of Reduced and Spent Catalysts. Figure 5A shows the XRD patterns of freshly reduced NFA catalysts for 2θ = 42–48°. All of the patterns in Figure 5A show a diffraction peak corresponding to the Ni metal phase that is centered at around 2θ = 44.5°. However, a gradual shift to smaller angle was observed for the patterns of NFA(500) and NFA(700) catalysts. According to previous reports,[34] the shift is interpreted to result from the creation of defect sites in the metallic Ni phase by Fe species, thus resulting in the formation of a Ni-rich Ni–Fe alloy with a face-centered-cubic (fcc) structure. The average particle size of metallic Ni was determined by broadening of the (111) line of nickel at around 44.5°. The Ni particle sizes were estimated to be 18.6, 21.7, and 22.7 nm for NFA(500), NFA(700), and NFA(900), respectively (Table 3). The average Ni particle sizes were found to increase with increasing calcination temperature, and this can be primarily attributed to the decrease in the surface area of the corresponding Fe–Al support. In addition to the peaks belonging to metallic Ni, all of the profiles show a peak at around 2θ = 43.5°, which is assigned to an Fe-rich Ni–Fe alloy with fcc structure.[35] The average particle size of the Ni–Fe alloy phase was estimated at 2θ = 43.5° and was observed to decrease with decreasing calcination temperature of the NFA catalyst supports. Furthermore, the broadness of the Ni–Fe alloy peak suggests that the Fe and Ni composition during alloy phase formation is not uniform. Together with the TPR results (which will be presented later in Figure 6), the results reveal that reduced Fe species can interact with reduced Ni species to form Ni–Fe bimetallic compounds. On the other hand, the

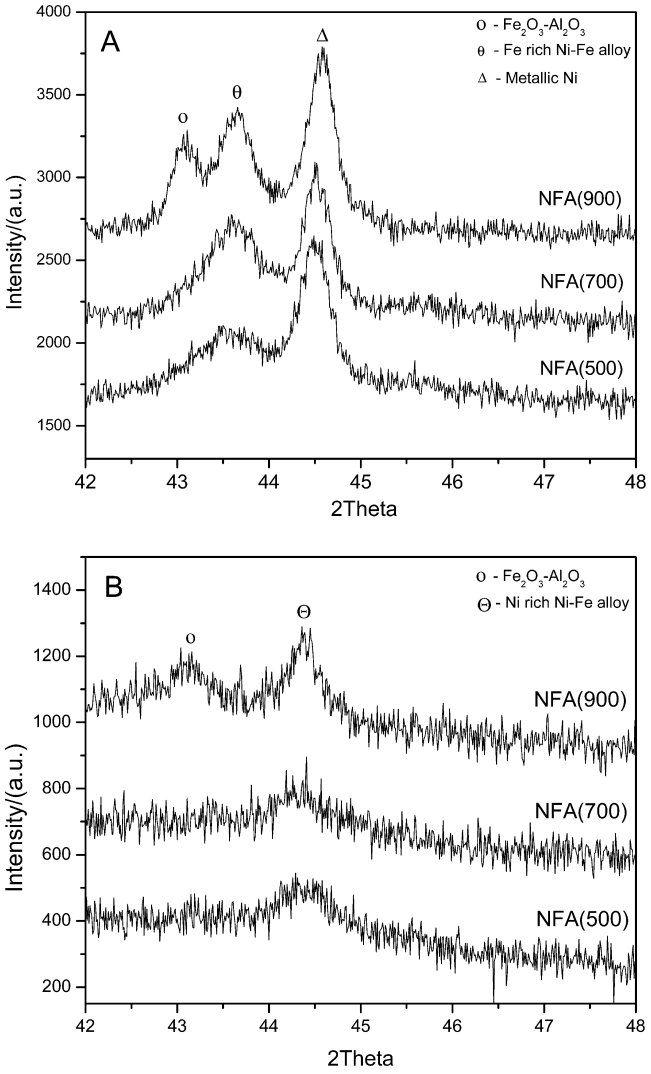

Figure 5. XRD patterns of (A) freshly reduced and (B) spent Fe_2O_3–Al_2O_3-supported Ni catalysts.

XRD pattern of NFA(900) in Figure 5A has peak at around 2θ = 43.1° that is assigned to the Al_2O_3-rich Fe_2O_3 corundum phase.[26] This phase is relatively inert, thereby inferring that it is hard to reduce and thermally stable. It is noteworthy to mention here that a peak at 2θ = 33.2° corresponding to an Fe_2O_3-rich Fe_2O_3–Al_2O_3 hematite phase[36] was observed in the XRD patterns of freshly calcined NFA catalysts. However, this peak disappeared in XRD patterns of the reduced NFA catalysts. The bulk compositions of Ni–Fe alloy in the reduced NFA catalysts presented in Table 3 were determined using Vegard's rule.[24] The Fe/Ni molar ratios are in the order of 1.28, 1.22, and 0.98 for NFA(500), NFA(700), and NFA(900) catalysts, respectively. This suggests that the reduced NFA(500) catalyst had a slightly higher Fe-rich Ni–Fe alloy phase than other NFA catalysts. The presence of Ni–Fe bimetallic compounds on the NFA catalysts was also confirmed after a life test for 6 h, as shown in Figure 5B. It can be observed from Figure 5B that the peak intensities appeared to be considerably lower than the XRD patterns of corresponding reduced NFA catalysts. This is possibly due to the deposition of amorphous carbon species over the NFA catalysts during the SRT process. In comparison with the XRD patterns of reduced NFA catalysts (Figure 5A), the peak assigned to the Fe-rich

dx.doi.org/10.1021/cs400621p | ACS Catal. 2014, 4, 289–301

Table 3. Ni−Fe Alloy Crystallite Sizes for Reduced and Spent NFA Catalysts

	reduced				spent		
	metallic Ni phase		Fe-rich Ni−Fe alloy phase		Ni-rich Ni−Fe alloy phase		
catalyst	2θ (deg)	crystallite size (nm)	2θ (deg)	crystallite size (nm)	2θ (deg)	crystallite size (nm)	Fe/Ni atomic ratio[a]
NFA(500)	44.45	18.6	43.56	07.7	44.34	10.6	1.28
NFA(700)	44.48	21.7	43.58	11.3	44.37	11.8	1.22
NFA(900)	44.53	22.7	43.59	16.8	44.39	19.3	0.80

[a]Calculated from the $d(200)$ spacing from XRD patterns of reduced catalysts using Vegard's law: $d_{Ni-Fe} = d_{Ni} \times Ni/(Ni + Fe) + d_{Fe} \times Fe/(Ni + Fe)$, where d_{Ni} and d_{Fe} are 0.1762 nm (JCPDS no. 01-070-1849) and 0.1823 nm (JCPDS no. 01-089-4185), respectively.

Ni−Fe alloy phase was weakened and almost vanished. Correspondingly, the peak assigned to the metallic Ni phase in Figure 5A was also weaker and shifted to lower angles. This shifted peak observed in Figure 5B can be assigned to a Ni-rich Ni−Fe alloy phase (at 2θ = 44.3°). In addition, this shift to lower angles suggests that the bulk composition of Fe to Ni can increase.[22] The average particle sizes of this Ni-rich Ni−Fe alloy phase were determined at around 2θ = 44.3° and were observed to be 10.6, 11.8, and 19.3 nm for the NFA(500), NFA(700), and NFA(900) catalysts, respectively. According to the particle size values in Table 3, the average Ni metal size for spent catalysts generally decreased during SRT reaction. The decrease in the particle size was comparatively higher for the Ni/Fe−Al(500) catalyst than others. This behavior is mainly due to the presence of the higher amount of Fe species in the catalysts, which plays an important role in forming the Ni−Fe alloy phase. The decrease in Ni particle size for the spent catalysts is possibly due to the formation of a reasonably low crystalline Ni-rich Ni−Fe alloy phase during the SRT process at a reaction temperature of 650 °C.

3.2.4. H_2-TPR Analysis. Generally, the reduction behavior of any bimetallic catalyst is a complex phenomenon. Likewise, for Ni−Fe catalysts, its complexity is derived from the multiple interactions that can arise during the catalyst preparation process as well as the multiple reduction centers that Fe species possess. However, in order to better understand the reduction behavior of NFA catalysts, TPR profiles for an Al_2O_3-supported Ni catalyst [NA(500)] up to 1000 °C were obtained, and the profiles are presented in Figure 6. The TPR profile of NA(500) shows a two-stage reduction behavior. A lower-intensity, lower-temperature reduction peak centered at ∼450 °C is due to the reduction ($Ni^{2+} \rightarrow Ni^0$) of NiO species not interacting with the Al_2O_3 support. On the other hand, the major reduction peak starting from 650 to 1000 °C is due to the reduction of Ni species present in $NiAl_2O_4$ spinel.[36] In contrast, the TPR profiles of the NFA(x) catalysts have three reduction centers. First, a low-temperature reduction peak ranging from 250 to 500 °C and centered at 460 °C can be attributed to the reduction of Fe species (Fe_2O_3 to Fe_3O_4).[36] According to both the literature[37] and the TPR profile of NA(500), uninteracted Ni species were also reduced in this reduction temperature range. However, because of the presence of alumina in the γ phase, these Ni species are expected to have strong interactions with support elements under the present catalyst preparation conditions. This suggests that the low-temperature reduction peak is mainly due to the reduction of Fe species. Second, a moderate-temperature reduction peak ranging from 500 to 800 °C can be assigned to the conversion (to Ni^0) of NiO species that have interacted with Fe species. According to previous reports,[38] in Ni−Fe bimetallic catalysts, the Ni reduction center shifts to higher temperature with an increase in the interaction with Fe species in the catalyst. The TPR profile of the NFA(900) catalyst suggests that it has weaker Ni−Fe interactions than the other catalysts. The weaker Ni−Fe interactions in the NFA(900) catalyst exist because the support material of the NFA(900) catalyst was calcined at 900 °C prior to preparing the supported Ni catalyst. This calcination temperature of 900 °C is sufficient to establish strong interactions between Fe and Al species in the support to form an inert corundum $Fe_2O_3-Al_2O_3$ phase. The formation of this inert phase was previously shown in Figure 5A,B for the NFA(900) catalyst. Lastly, all of the NFA samples have a high-temperature reduction peak starting from 750 to 1000 °C, which can be attributed to the reduction of Ni species in $NiAl_2O_3$ spinel. The same reduction center is also observed in the TPR profile of the NA(500) catalyst. This high-temperature reduction peak is more significant for NFA(500) than for the other catalysts. However, in the TPR profile of the NFA(900) catalyst, this peak appears to be a shoulder of the moderate-temperature reduction peak. Finally, TPR analysis suggested that Ni species in the NFA(500) catalyst have stronger interactions with support species (Fe and Al species) compared with the other catalysts.

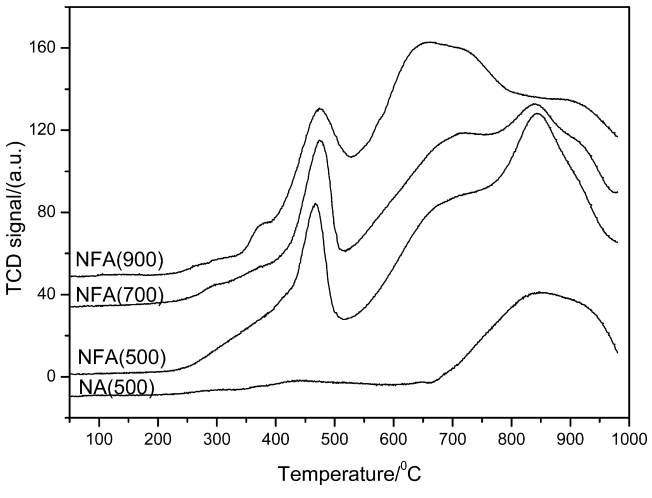

Figure 6. H_2-TPR profiles of the NA(500) and NFA(x) catalysts.

3.2.5. H_2-TPR$_1$ and H_2-TPR$_2$ Study. The reduction behavior of the NFA catalysts up to 1000 °C is presented in Figure 6. However, according to the SRT performance conditions reported in section 2.3, all of the catalysts underwent reductive treatment at 700 °C for 1 h prior to use in the SRT process. Thus, in order to understand the actual reduced species involved in the SRT reaction, several consecutive TPSR studies were conducted on fresh NFA catalysts using 5% H_2/N_2 and 5% O_2/N_2 gases. The thus-obtained TPR$_1$ and TPR$_2$ profiles for the NFA(x) catalysts are depicted in Figure 7. The TPR$_1$

dx.doi.org/10.1021/cs400621p | ACS Catal. 2014, 4, 289−301

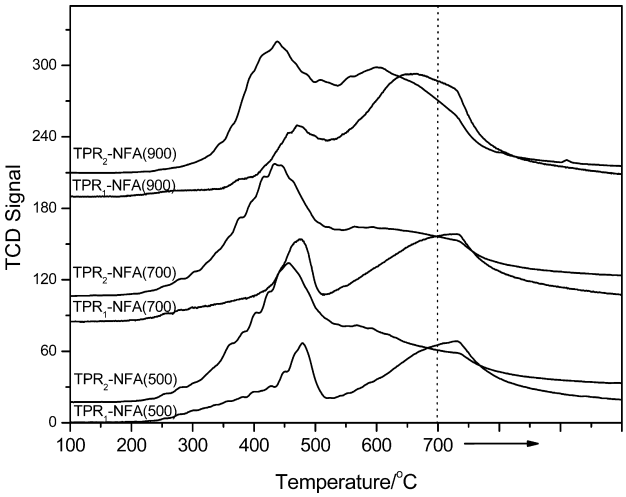

Figure 7. H_2-TPR_1 and H_2-TPR_2 profiles of Ni supported on Fe_2O_3–Al_2O_3 supports calcined at different temperatures.

profiles for all of the NFA catalysts in Figure 7 show two reduction peaks. According to conclusions made from Figure 6, the low-temperature reduction peak at ∼470 °C is due to reduction of Fe species ($Fe_2O_3 \rightarrow Fe_3O_4$) as well as uninteracted Ni species ($NiO \rightarrow Ni^0$), whereas the high-temperature peak centered at ∼700 °C corresponds to conversion of Ni species that have strongly interacted with Fe species. Interestingly, this low-temperature reduction peak was also observed in the TPR_2 profiles for all of the NFA catalysts. However, this low-temperature peak shifted by ∼30 °C to an even lower temperature region, and the H_2 consumption for this peak increased significantly compared with its corresponding TPR_1 profile. On the other hand, the total H_2 consumption values for NFA catalysts during the TPR_1 and TPR_2 processes (Table 2) show that H_2 consumption value during TPR_2 was generally higher than that during TPR_1. This increase in the H_2 consumption was greater for the NFA(500) catalyst than for the other catalysts. This increase is possibly due to redispersion of reduced species upon exposure to the oxygen environment. According to previous reports,[22] during the TPR_1 process Fe species were reduced first, and these reduced Fe species can interact intimately with Ni species to form Ni–Fe alloy species. The thus-formed Ni–Fe alloy species were oxidized during the TPO process and then reduced at lower temperature during the TPR_2 step. Since some or most of the Ni species were involved in forming Ni–Fe alloy species, the involved Ni species were also reduced in this low-temperature region. Furthermore, a significant high-temperature reduction peak (∼600 °C) due to the reduction of Ni species that had interacted with Fe species was observed in the TPR_2 profile of the NFA(900) catalyst. This high-temperature reduction peak was broader and appeared like a shoulder on the low-temperature reduction peak in the TPR_2 profiles of the NFA(500) and NFA(700) catalysts. It is noteworthy to mention here that the H_2 consumption for the high-temperature reduction peak for all of the TPR_2 profiles is comparatively lower than that for the TPR_1 profiles. Finally, these consecutive surface reaction experiments suggest that the amount of reduced Ni species from TPR_1 that were involved in forming Ni–Fe alloy species was higher for the NFA(500) and NFA(700) catalysts than for the NFA(900) catalyst. They also confirm that the active components available to perform the SRT reaction were mostly Ni–Fe alloy species in all of the catalysts.

3.2.6. Temperature-Programmed Surface Reaction with Toluene and Water. TPSR studies with water and toluene were measured separately over reduced NFA catalysts in order to understand the nature of the active centers and their capability to activate reactant molecules, namely, water and toluene. The TPSR study was also carried out over the NA(500) catalyst for comparison. TPSR of toluene was carried out over reduced NA(500) and NFA catalysts, and the results are depicted in Figure 8A,B as H_2 and CO evolution as

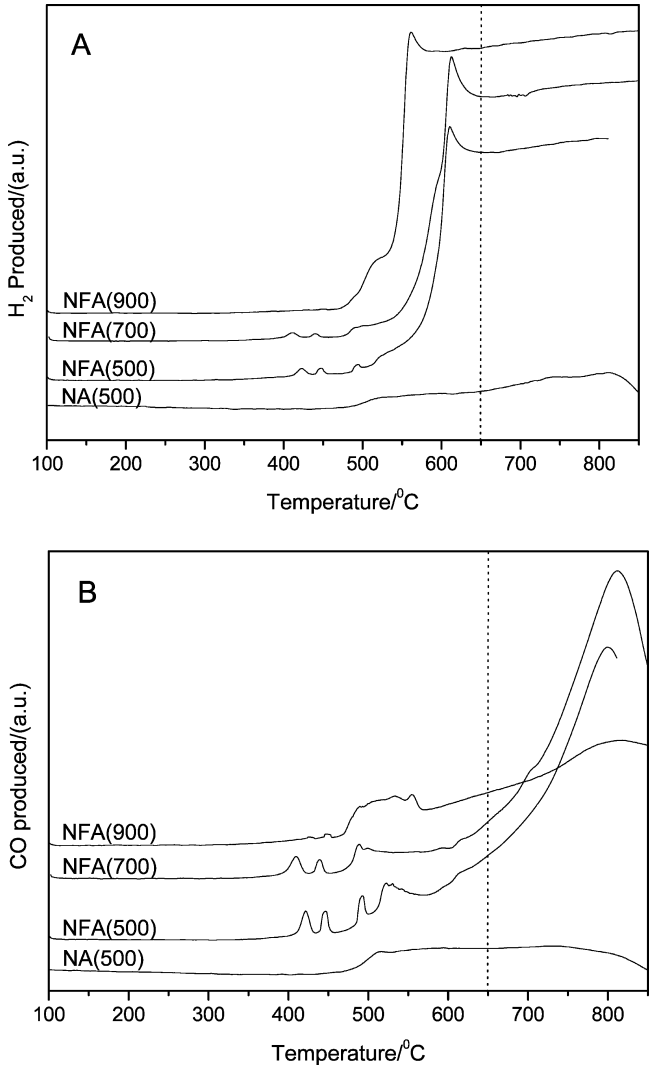

Figure 8. TPSR with toluene over NA(500) and NFA catalysts: (A) H_2 produced and (B) CO produced as functions of temperature.

functions of temperature, respectively. Two gaseous products, H_2 and CO, were observed during the TPSR of toluene, along with solid carbon that was deposited on the catalyst. This product distribution can be explained by eqs 10 and 11:[39]

$$M^* + C_7H_8 \rightarrow M^*C + H_2 \quad (10)$$

$$M^*C + S{-}O \rightarrow M^* + S + CO \quad (11)$$

where M* is an active metal center (Ni^0 or Ni–Fe alloy) and S–O is a lattice oxygen species present in the NFA catalyst. From Figure 8A, H_2 was produced from toluene decomposition

dx.doi.org/10.1021/cs400621p | ACS Catal. 2014, 4, 289–301

according to eq 6. This decomposition started at around 470 °C in all of the profiles. However, the rate of H_2 production was higher for NFA catalysts than for the NA(500) catalyst. Similarly, CO was also produced during TPSR of toluene according to eq 11. The CO production, as shown in Figure 8B, also began at around 470 °C in all of the profiles. However, the amount of CO produced seemed to be less for the NFA(900) and NA(500) catalysts compared with the NFA(500) and NFA(700) catalysts. According to eq 11, CO production depends on the amount of available lattice oxygen species, possibly from the support in the catalyst during TPSR of toluene. This suggests that NFA(500) and NFA(700) catalysts have higher amounts of lattice oxygen species available to achieve better performance in the SRT reaction than the NFA(900) catalyst.

Subsequently, TPSR of water was also carried out over reduced NA(500) and NFA catalysts. Figure 9 shows the H_2 evolution as a function of temperature during TPSR with water over the NA(500) and NFA(x) catalysts. In the TPSR with water experiments, only H_2 evolved, and this can be explained according to eqs 12 and 13:

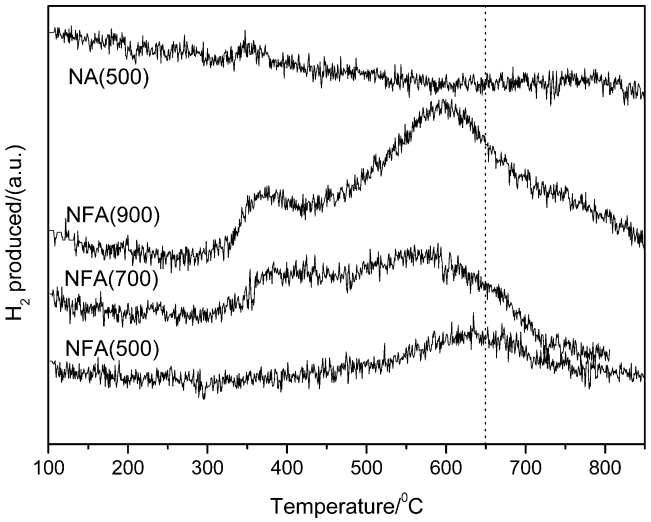

Figure 9. H_2 produced during TPSR with water over NA(500) and NFA catalysts.

$$M^* + H_2O \rightarrow H_2 + M^*O \quad (12)$$

$$M^*O + S \rightarrow M^* + S{-}O \quad (13)$$

where M* is an active metal center (Ni^0 or Ni−Fe alloy) and S is an oxygen-vacant center in the support.

Generally, in the NA(500) catalyst, only metallic Ni species possess available active sites to activate water molecules. However, in the NFA catalysts, in addition to metallic Ni, Ni−Fe alloy species also exist to activate water molecules in order to generate H_2 gas. In Figure 9, NA(500) shows a single H_2 evolution peak starting from 310 °C and centered at 370 °C. This H_2 evolution peak is solely due to active sites found on metallic Ni. A similar H_2 evolution peak can also be observed in all of the other profiles shown in Figure 9. However, the intensities of those H_2 evolution peaks differ from each other, and it is also observed that this H_2 evolution peak shifts to higher temperature in going from NFA(900) to NFA(500). In addition, a high-temperature H_2 peak is also observed in the TPSR profiles of all NFA catalysts starting from 450 °C; this peak is centered at 600 °C in the TPSR profiles of the NFA(700) and NFA(900) catalysts and at 650 °C in the TPSR profile of the NFA(500) catalyst. However, the intensities of these peaks vary. From the TPSR profile of the NFA(500) catalyst, it is evident that maximum H_2 evolution occurs at 650 °C, coinciding with the actual temperature at which the SRT reaction was conducted in the present study. This ability to evolve the highest quantity of H_2 at 650 °C is one of the reasons why the NFA(500) catalyst is superior over other catalysts. Combining the results obtained from Figures 8 and 9 shows that the superiority of the NFA(500) catalyst over the others is due to the existence of higher amounts of available oxygen species during the SRT reaction as well as its ability to maximize water splitting at a temperature at which the SRT reaction is conducted (i.e., 650 °C). On the contrary, despite the ability of the NFA(900) catalyst to split water at a lower temperature than the others, it has a lower catalytic performance because of the lower amount of available oxygen species in the catalyst. As will be shown subsequently in TPO of spent catalysts, the lower oxygen availability results in a higher amount of graphitic carbon deposition on the NFA(900) catalyst.

3.2.7. CO-Pulse Chemisorption. The amount of active metal content in the freshly reduced NFA catalysts was measured using CO pulse titration at 0 °C as reported in the literature.[40] The CO uptake results presented in Table 2 were found to be 19.15, 18.23, and 15.97 μmol/g for the NFA(500), NFA(700), and NFA(900) catalysts, respectively. Since Ni is the main active component in the present steam reforming reaction, an intrinsic rate per metal site (turnover frequency, TOF) for the NFA catalysts during the SRT reaction was evaluated by considering the toluene conversions shown in Table 1 as well as the CO uptake results presented in Table 2. The TOF values of the NFA(500), NFA(700) and NFA(900) catalysts are 4.4, 3.9, and 3.1 s^{-1}, respectively. From these TOF values, it is clearly observed that the NFA(500) catalyst has a higher TOF than the other NFA catalysts. On the other hand, dispersion values of 1.12, 1.07, and 0.93% were obtained for the NFA(500), NFA(700), and NFA(900) catalysts, respectively. Thus, the TOF value was highest for NFA(500) catalyst even though it has the highest CO consumption value among all the catalysts. This result affirms that the better performance of NFA(500) can be attributed to the presence of a higher amount of surface active metal species.

3.2.8. XPS Analysis of Reduced and Spent Catalysts. A comparative XPS study was done in order to understand the surface species present in the freshly reduced and spent NFA catalysts. Figure 10 displays the binding energies (BEs) of Ni $2p_{3/2}$ species present in the NFA catalysts. Generally, the BE of metallic Ni 2p is 852.4 ± 0.4 eV, the BE of Ni 2p in NiO is 854 ± 0.4 eV, the BE of Ni 2p in $NiFe_2O_4$ is 855 ± 0.4 eV, and the BE of Ni 2p in $NiAl_2O_4$ is around 857 ± 0.4 eV.[41] Figure 10A shows Ni 2p BEs present in reduced NFA catalysts due to the presence of Ni^0 (~852.2 eV) and Ni^{2+} (~855 eV) species, where the Ni^{2+} species interacts with Fe species present in the NFA(x) catalysts. According to Figure 10A, moving from the profile of NFA(500) to that of NFA(900), both BE values of Ni 2p shifted slightly to lower values. This indicates that Ni species present in NFA(900) catalyst have weaker interactions with Fe species when compared with those in the NFA(700) and NFA(500) catalysts, affirming the observations in the TPR profiles presented in Figure 6. Next, Ni 2p BEs of spent NFA(x) catalysts are displayed in Figure 10B, which shows the

dx.doi.org/10.1021/cs400621p | ACS Catal. 2014, 4, 289−301

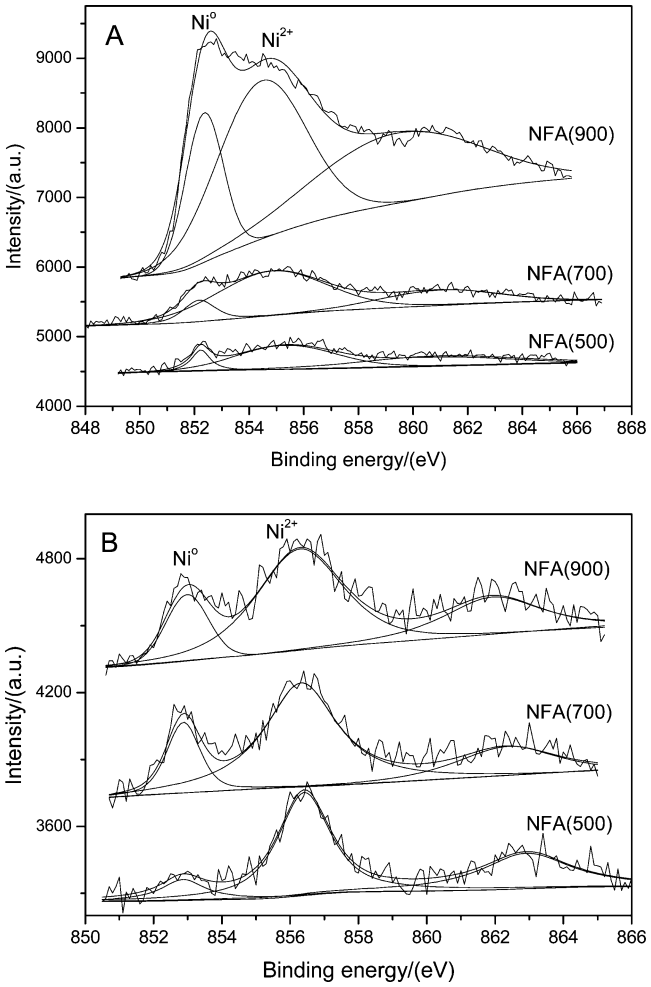

Figure 10. Ni 2p binding energies of (A) freshly reduced and (B) spent NFA catalysts.

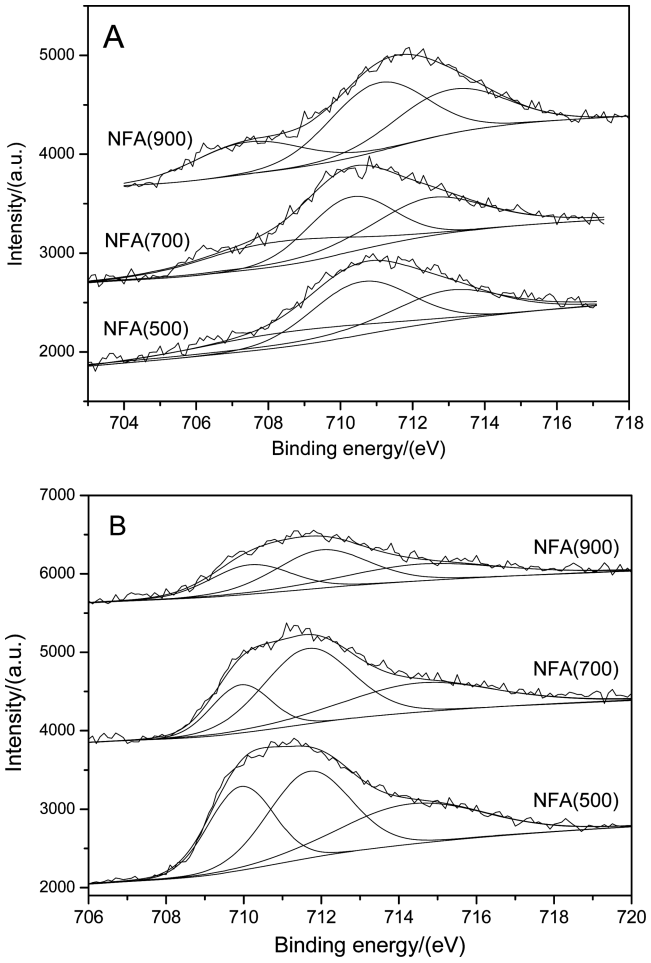

Figure 11. Fe 2p binding energies of (A) freshly reduced and (B) spent NFA catalysts.

presence of two kinds of Ni species, namely, Ni^0 (BE at 852.8 eV) and Ni^{2+} (BE at 856.3 eV). All of the Ni 2p BEs of spent catalysts were shifted to higher values compared with the Ni 2p BE values observed in Figure 10A. This shift to higher BE values in all of the spent NFA catalysts indicates that the interactions between Ni species and support species were significantly enhanced during the reforming process. This hypothesis was further supported by the XRD patterns of spent NFA catalysts as presented in Figure 5B.

Figure 11 displays BEs of Fe $2p_{3/2}$ species present in reduced and spent NFA catalysts. Unlike Ni species, Fe species in NFA catalysts can exist in multiple oxidation states ranging from +3 to 0, and thus, it can be a challenge to identify the exact oxidation states of Fe species present in NFA catalysts. The following interpretation of the BEs of Fe 2p in Figure 11 was derived after consideration of numerous literature reports. Figure 11A, which depicts Fe 2p BEs of reduced NFA catalysts, shows Fe 2p BE values of 707 ± 0.2 and 711 ± 0.2 eV, which correspond to Fe^0 species and Fe species in Fe_3O_4 form, respectively. However, according to the literature,[41] the latter Fe 2p BE also corresponds to Fe species that have interacted with Ni species in NFA(x) catalysts. In addition, compared with other catalysts, the shift to higher BE values of around 711 eV in the NFA(900) catalyst is possibly due to stronger interactions of Fe species with Al species. This was further confirmed through the presence of the corundum (Fe_2O_3–Al_2O_3) phase observed in the XRD pattern of the NFA(900) catalyst (Figure 5). Next, Fe 2p BEs of spent NFA catalysts are displayed in Figure 11B. The BE values at around 710 ± 0.2 eV correspond to Fe species in FeO form, while BE values at 712 ± 0.2 eV can be attributed to Fe species present in Fe_3O_4 form as well as Fe species that are interacted with Ni species. It is also evident that this BE value is shifted to a slightly higher value for the NFA(900) catalyst compared with the other catalysts. This is due to the stronger interaction of Fe species with Al species in the catalytic support, resulting in a shift similar to that previously observed in Figure 11A. On comparison with Figure 11A, the absence of Fe 2p BE values around 707 eV in Figure 11B, corresponding to Fe^0 species, suggests the exhibition of redox behavior. During the SRT process, the Fe^0 species present in reduced NFA catalysts are partially oxidized to form intermediary FeO species, which have a better redox nature than both Fe^0 and Fe_3O_4 species. This redox behavior enables Fe species to easily shuffle between their oxidation states to enhance the reforming process by providing necessary oxygen species to active Ni species.

The molar composition of various surface species present in freshly reduced and spent NFA catalysts are presented in Table 4. It is noteworthy to mention here that the bulk compositions of all of the NFA catalysts were similar. However, it can be observed from Table 4 that the Fe/Ni molar ratios on the surfaces of the reduced NFA(500), NFA(700), and NFA(900) catalysts were 1.56, 0.74, and 0.38 respectively, suggesting that

dx.doi.org/10.1021/cs400621p | ACS Catal. 2014, 4, 289–301

Table 4. Surface Compositions of Elements Present in Reduced and Spent NFA Catalysts

		surface composition (%)						
catalyst	form	Ni^0	Ni^{2+}	Fe^0	Fe^{x+}	Al	O	Fe/Ni surface atomic ratio
NFA(500)	reduced	0.27	1.02	0.77	1.25	35.46	65.21	1.56
NFA(500)	spent	0.20	1.07	–	6.85	59.59	31.92	5.39
NFA(700)	reduced	0.44	2.75	1.04	1.33	30.29	64.14	0.74
NFA(700)	spent	0.40	1.65	–	6.69	60.49	30.73	3.20
NFA(900)	reduced	3.96	9.84	1.84	3.47	23.62	57.27	0.38
NFA(900)	spent	0.48	2.08	–	5.32	65.00	27.11	2.07

the reduced NFA(500) catalyst is rich with surface Fe species. On the other hand, the Fe/Ni molar ratio of spent NFA catalysts suggests that during the course of the SRT reaction all of the catalysts were enriched with Fe species. Furthermore, it can be observed that there was a significant increase in the surface Al species on the spent NFA catalysts compared with the reduced NFA catalysts. However, this increment is considerably lower for the NFA(500) catalyst than for the others. In addition, the surface O species were decreased in the spent NFA catalysts compared with their corresponding reduced ones, suggesting that this decrease in surface oxygen species is possibly due to their involvement in the steam reforming process. It is well-known that metallic Ni catalysts are widely explored for steam reforming of hydrocarbons because metallic Ni has a strong ability to activate C−H and C−C bonds in the hydrocarbon molecules on the Ni metal surface.[42] According to Table 4, the amount of surface metallic Ni species is lower in the spent NFA catalysts than in the reduced catalysts. This decrease in metallic Ni species is possibly due to the increase in surface Fe species that can encapsulate metallic Ni species during SRT process with time on stream. Additionally, the deposition of carbon can also be responsible for the decrease of metallic Ni species during the SRT process, suggesting that the deactivation behavior of all NFA catalysts with time on stream during the SRT process (Figure 1) is primarily due to the decrease in the amount of metallic Ni species. Finally, the better catalytic performance of NFA(500) catalysts is attributed to the presence of strong interactions between Ni and Fe species to form Ni−Fe alloy particles that are rich in surface Fe species. This extra Fe species are mostly partially reduced Fe^{2+} species, which are highly redox-active in nature.

3.2.9. TGA of Spent Catalysts. The amounts of carbon deposited over spent NFA catalysts after SRT at 650 °C for 6 h were measured using TGA up to 1000 °C in air, and the results are presented in Table 5. According to Table 5, the carbon deposition rates are 21.2, 18.3, and 48.9 $mg_C\ g_{cat}^{-1}\ h^{-1}$ for the NFA(500), NFA(700), and NFA(900) catalysts, respectively. Overall, the NFA(900) catalyst has the highest carbon deposition rate among all of the catalysts. The high carbon deposition rate could be one of the reasons accounting for its lower SRT performance. According to the literature,[43] the deposited carbon can encapsulate the active metal components during the SRT reaction, thereby leading to deactivation of the catalyst by decreasing the number of active metal sites presented by the catalyst. Despite having a higher carbon formation rate than the NFA(700) catalyst, the NFA(500) catalyst achieved more superior catalytic performance than the NFA(700) catalyst. The reason for this can be explained on the basis of the nature of the carbon species deposited during the SRT reaction, as presented in the next section.

Table 5. Carbon Deposition Rates for Spent NFA(x) Catalysts As Determined by TGA Analysis[a]

catalyst	carbon deposition rate ($mg_C\ g_{cat}^{-1}\ h^{-1}$)
NFA(500)	21.2
NFA(700)	18.3
NFA(900)	48.9

[a]Reaction conditions: reaction temperature = 650 °C; reaction time = 6 h; toluene = 188 μmol min^{-1}; steam = 4444 μmol min^{-1}; He = 5357 μmol min^{-1}; W = 30 mg.

3.2.10. TPO of Spent Catalysts. Figure 12 displays the TPO profiles (CO_2 emission plotted against the oxidation temperature) of carbon deposited on spent NFA catalysts after SRT at 650 °C for 6 h. The oxidation of carbonaceous species starts at around 400 °C for almost all of the catalysts. The asymmetric shape of the CO_2 peaks for all of the catalysts implies the presence of several different carbonaceous species. Generally, unsaturated hydrocarbons such as olefins and graphitic and filamentous carbon tend to oxidize at higher temperatures compared with hydrocarbons with saturated C−C bonds such as paraffinic and amorphous carbon.[44] From the profiles, both amorphous carbons ($T_{oxidation}$ < 650 °C) and graphitic/filamentous carbon ($T_{oxidation}$ > 650 °C) can be found in all of the spent catalysts. According to Figure 12, the profile of the NFA(900) catalyst has a single oxidation peak centered at T_{max} ≈ 710 °C with most of the carbons being oxidized after 650 °C,

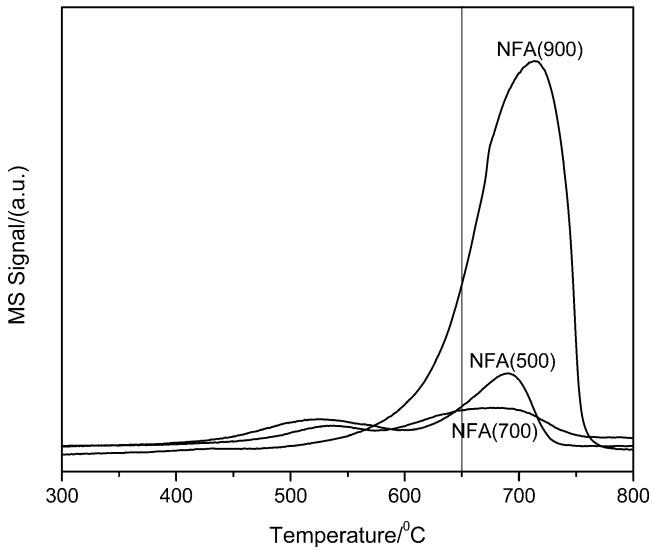

Figure 12. TPO profiles of spent NFA catalysts. Reaction conditions: toluene = 188 μmol min^{-1}; steam = 4444 μmol min^{-1}; He = 5357 μmol min^{-1}; W = 30 mg; reaction temperature = 650 °C; reaction time = 6 h.

dx.doi.org/10.1021/cs400621p | ACS Catal. 2014, 4, 289−301

whereas for the NFA(500) and NFA(700) catalysts, the profiles show two stages of oxidation behavior with a low-temperature peak centered at $T_{max} \approx 525$ and 535 °C, respectively, as well as a high-temperature peak centered at $T_{max} \approx 690$ and 680 °C, respectively. Furthermore, most of the deposited carbon was oxidized below 650 °C for both the NFA(500) and NFA(700) catalysts. This could be one of the reasons for the lower amount of carbon deposited on NFA(500) and NFA(700) catalysts compared with the NFA(900) catalyst during the SRT reaction. According to other studies,[43] this amorphous carbon can be easily reformed compared with graphitic carbon during the SRT process at 650 °C. On the contrary, the superior SRT performance of NFA(500) over NFA(700) catalyst despite its higher carbon formation rate can possibly be attributed to the fact that its low-temperature oxidation peak is centered at a lower temperature than that of NFA(700) catalyst.

4. CONCLUSIONS

Iron−alumina-supported nickel−iron alloy catalysts were explored for steam reforming of toluene as a biomass tar model compound. The NFA(500) catalyst showed the best steam reforming performance in terms of higher catalytic activity and stability for 26 h reaction time with a H_2/CO value of 4.5. The superior catalytic performance of NFA(500) is mainly due to the presence of a higher amount of surface active metal species, Fe-rich Ni−Fe alloy particles, strong metal−support interactions, and a relatively low carbon deposition rate. The high catalyst surface area and higher amount of available lattice oxygen species also play important roles in promoting the reforming activity of the NFA(500) catalyst over the others. The synergy between Ni and Fe atoms is achieved by forming Fe-rich Ni−Fe alloy particles, which are crucial for the high activity of the NFA(500) catalyst. In addition, the strong interaction between metal and support on the NFA(500) catalyst can prevent metal sintering, thus achieving high catalytic stability. Finally, this NFA(500) catalyst has great potential for application in the steam reforming of biomass tar.

AUTHOR INFORMATION

Corresponding Author

*Address: Department of Chemical and Biomolecular Engineering, National University of Singapore, Singapore 119260, Republic of Singapore. Tel.: +65 6516 6312. Fax: +65 6779 1936. E-mail: chekawis@nus.edu.sg.

Notes

The authors declare no competing financial interest.

ACKNOWLEDGMENTS

The authors gratefully thank National University of Singapore and the National Environmental Agency (NEA-ETRP Grant 1002114 and RP 279-000-333-490) for generously supporting this work.

REFERENCES

(1) Huber, G. W.; Iborra, S.; Corma, A. *Chem. Rev.* **2006**, *106*, 4044−4098.
(2) Hu, X.; Lu, G. *Appl. Catal., B* **2009**, *88*, 376−385.
(3) Dauenhauer, P. J.; Dreyer, B. J.; Degenstein, N. J.; Schmidt, L. D. *Angew. Chem.* **2007**, *119*, 5968−5971.
(4) Serrano, D. P.; Aguado, J.; Escola, J. M. *ACS Catal.* **2012**, *2*, 1924−1941.
(5) Dapsens, P. Y.; Mondelli, C.; Ramirez, J. P. *ACS Catal.* **2012**, *2*, 1487−1499.
(6) De Lasa, H.; Salaices, E.; Mazumder, J.; Lucky, R. *Chem. Rev.* **2011**, *111*, 5404−5433.
(7) Swierczynski, D.; Libs, S.; Courson, C.; Kiennemann, A. *Appl. Catal., B* **2007**, *74*, 211−222.
(8) Polychronopoulou, K.; Giannakopoulos, K.; Efstathiou, A. M. *Appl. Catal., B* **2012**, *111*, 360−375.
(9) Guell, B. M.; Babich, I.; Nichols, K. P.; Gardeniers, J. G. E.; Lefferts, L.; Seshan, K. *Appl. Catal., B* **2009**, *90*, 38−44.
(10) Kimura, T.; Miyazawa, T.; Nishikawa, J.; Kado, S.; Okumura, K.; Miyao, T.; Naito, S.; Kunimori, K.; Tomishige, K. *Appl. Catal., B* **2006**, *68*, 160−170.
(11) Wang, L.; Hisada, Y.; Koike, M.; Li, D.; Watanabe, H.; Nakagawa, Y.; Tomishige, K. *Appl. Catal., B* **2012**, *121−122*, 95−104.
(12) Guan, G.; Chen, G.; Kasai, Y.; Lim, E. W. C.; Hao, X.; Kaewpanha, M.; Abuliti, A.; Fushimi, C.; Tsutsumi, A. *Appl. Catal., B* **2012**, *115−116*, 159−168.
(13) Ammendola, P.; Cammisa, E.; Chirone, R.; Lisi, L.; Ruoppolo, G. *Appl. Catal., B* **2012**, *113−114*, 11−18.
(14) Virginie, M.; Courson, C.; Niznansky, D.; Chaoui, N.; Kiennemann, A. *Appl. Catal., B* **2010**, *101*, 90−100.
(15) Kuhn, J. N.; Zhao, Z.; Felix, L. G.; Slimane, R. B.; Choi, C. W.; Ozkan, U. S. *Appl. Catal., B* **2008**, *81*, 14−26.
(16) Mei, D.; Lebarbier, V. M.; Rousseau, R.; Glezakou, V. A.; Albrecht, K. O.; Kovarik, L.; Flake, M.; Dagle, R. A. *ACS Catal.* **2013**, *3*, 1133−1143.
(17) Nakamura, K.; Miyazawa, T.; Sakurai, T.; Miyao, T.; Naito, S.; Begum, N.; Kunimori, K.; Tomishige, K. *Appl. Catal., B* **2009**, *86*, 36−44.
(18) Li, D.; Wang, L.; Koike, M.; Nakagawa, Y.; Tomishige, K. *Appl. Catal., B* **2011**, *102*, 528−538.
(19) Maluf, S. S.; Assaf, E. M. *Fuel* **2009**, *88*, 1547−1553.
(20) Wu, P.; Li, X.; Ji, S.; Lang, B.; Habimana, F.; Li, C. *Catal. Today* **2009**, *146*, 82−86.
(21) Miyazawa, T.; Kimura, T.; Nishikawa, J.; Kado, S.; Kunimori, K.; Tomishige, K. *Catal. Today* **2006**, *115*, 254−262.
(22) Wang, L.; Li, D.; Koike, M.; Koso, S.; Nakagawa, Y.; Xu, Y.; Tomishige, K. *Appl. Catal., A* **2011**, *392*, 248−255.
(23) Wang, L.; Li, D.; Koike, M.; Watanabe, H.; Xu, Y.; Nakagawa, Y.; Tomishige, K. *Fuel* **2013**, *112*, 654−661.
(24) Koike, M.; Li, D.; Nakagawa, Y.; Tomishige, K. *ChemSusChem* **2012**, *5*, 2312−2314.
(25) Reed, T. B. *Free Energy of Formation of Binary Compounds*; MIT Press: Cambridge, MA, 1971; pp 66−70.
(26) Ishida, M.; Takeshita, K.; Suzuki, K.; Ohba, T. *Energy Fuels* **2005**, *19*, 2514−2518.
(27) Duprez, D. *Appl. Catal., A* **1992**, *82*, 111−157.
(28) Oemar, U.; Ang, P. S.; Hidajat, K.; Kawi, S. *Int. J. Hydrogen Energy* **2013**, *38*, 5525−5534.
(29) Ashok, J.; Kawi, S. *Int. J. Hydrogen Energy* **2013**, *38*, 13938−13949.
(30) Kechagiopoulos, P. N.; Voutetakis, S. S.; Lemonidou, A. A.; Vasalos, I. A. *Energy Fuels* **2006**, *20*, 2155−2163.
(31) Domine, M. E.; Iojoiu, E. E.; Davidian, T.; Guilhaume, N.; Mirodatos, C. *Catal. Today* **2008**, *133−135*, 565−573.
(32) Shi, Z.; Zhang, Z.; Fan, R.; Gao, M.; Guo, J. *J. Inorg. Organomet. Polym.* **2011**, *21*, 836−840.
(33) Chen, W.; Ding, Y.; Song, X.; Wang, T.; Luo, H. *Appl. Catal., A* **2011**, *407*, 231−237.
(34) Gheisari, K.; Javadpour, S.; Oh, J. T.; Ghaffari, M. *J. Alloys Compd.* **2009**, *472*, 416−420.
(35) Kuhrt, C.; Schultz, L. *J. Appl. Phys.* **1993**, *73*, 1975−1980.
(36) Kidambi, P. R.; Cleeton, J. P. E.; Scott, S. A.; Dennis, J. S.; Bohn, C. D. *Energy Fuels* **2012**, *26*, 603−617.
(37) Richardson, J. T.; Turk, B.; Twigg, M. V. *Appl. Catal., A* **1996**, *148*, 97−112.
(38) Tian, D.; Liu, Z.; Li, D.; Shi, H.; Pan, W.; Cheng, Y. *Fuel* **2013**, *104*, 224−229.
(39) Lamacz, A.; Krzton, A.; Mariadassou, G. D. *Catal. Today* **2011**, *176*, 347−351.

(40) Oyama, S. T.; Zhao, H.; Freund, H. J.; Asakura, K.; Wlodarczyk, R.; Sierka, M. *J. Catal.* **2012**, *285*, 1−5.
(41) *Handbook of X-ray Photoelectron Spectroscopy*; Wagner, C. D., Riggs, W. M., Davis, L. E., Moulder, J. F., Muilenberg, G. E., Eds.; Perkin-Elmer Corporation: Eden Prairie, MN, 1979; pp 76−80.
(42) Ahmed, S.; Aitani, A.; Rahman, F.; Al-Dawood, A.; Al-Muhaish, F. *Appl. Catal., A* **2009**, *359*, 1−24.
(43) Djinovic, P.; Crnivec, I. G. O.; Erjavec, B.; Pintar, A. *Appl. Catal., B* **2012**, *125*, 259−270.
(44) Gould, B. D.; Chen, X.; Schwank, J. W. *Appl. Catal., A* **2008**, *334*, 277−290.